Sierpiński Structure and Electronic Topology in Bi Thin Films on InSb(111)B Surfaces

Chen Liu,[1] Yinong Zhou,[2] Guanyong Wang,[3] Yin Yin,[1] Can Li,[1] Haili Huang,[1] Dandan Guan,[1,4] Yaoyi Li,[1,4] Shiyong Wang,[1,4] Hao Zheng,[1,4] Canhua Liu,[1,4] Yong Han,[5,6,*] James W. Evans,[5,6] Feng Liu,[2] and Jinfeng Jia[1,4,†]

[1]*Key Laboratory of Artificial Structures and Quantum Control (Ministry of Education), Shenyang National Laboratory for Materials Science, School of Physics and Astronomy, Shanghai Jiao Tong University, Shanghai 200240, China*

[2]*Department of Materials Science and Engineering, University of Utah, Salt Lake City, Utah 84112, USA*

[3]*Shenzhen Institute for Quantum Science and Engineering, Southern University of Science and Technology, Shenzhen 518055, China*

[4]*Tsung-Dao Lee Institute, Shanghai Jiao Tong University, Shanghai 200240, China*

[5]*Department of Physics and Astronomy, Iowa State University, Ames, Iowa 50011, USA*

[6]*Ames Laboratory, U.S. Department of Energy, Ames, Iowa 50011, USA*

(Received 27 November 2020; revised 11 February 2021; accepted 19 March 2021; published 30 April 2021)

Deposition of Bi on InSb(111)B reveals a striking Sierpiński-triangle (ST)-like structure in Bi thin films. Such a fractal geometric topology is further shown to turn off the intrinsic electronic topology in a thin film. Relaxation of a huge misfit strain of about 30% to 40% between Bi adlayer and substrate is revealed to drive the ST-like island formation. A Frenkel-Kontrova model is developed to illustrate the enhanced strain relief in the ST islands offsetting the additional step energy cost. Besides a sufficiently large tensile strain, forming ST-like structures also requires larger adlayer-substrate and intra-adlayer elastic stiffnesses, and weaker intra-adlayer interatomic interactions.

DOI: 10.1103/PhysRevLett.126.176102

The Sierpiński triangle (ST) [1] is a self-similar fractal with a fractional Hausdorff dimension $d_H = \log_2 3 = 1.584\,96\cdots$ and with fascinating mathematical properties [2]. Historically, such beautiful patterns were often utilized for aesthetic reasons, especially in architecture, e.g., on the medieval floors in Rome [3]. Many fundamental and intriguing phenomena in ancient and modern mathematics and physics, as well as computer science, are related to the STs, such as Pascal triangles [4], towers of Hanoi [5], chaos games [6], cellular automata [7], DNA computing [8,9], etc.

Theory and experiment have shown that fractal materials can exhibit plentiful and unusual thermal, mechanical, electric, electronic, electromagnetic, and optical properties which are often desirable for prospective nanodevice applications [10–16]. Fractal quasicrystals have even been predicted to possess nontrivial electronic topology usually pertained to crystals [17,18]. Recently, there has been also considerable interest in fabricating ST-like fractal materials, although the synthesis of such systems is notoriously difficult [19]. In 2014, a terpyridine-based architecture mimicking ST was synthesized in solution [20]. Subsequently, several research groups have successfully fabricated the fractal supramolecular materials featuring the ST pattern on the coinage metal surfaces: Ag(111) [21], Ag(100) [22], Au(111) [23–28], Au(100) [28,29], and Cu(111) [30], as well as on a graphite surface [31]. These fabricated fractal supramolecules can be organic, metal organic, CO compounds, etc., [16]. Theoretically, Monte Carlo simulations show that the formation of molecular STs in these systems is essentially related to directional intermolecular bonds [32,33].

As indicated above, previous fabrication of STs in experiments is by assembling small carbon-based molecules into supramolecules. There has not yet been any report of the synthesis for STs composed of single-element atoms. Obviously, experimental fabrication of such pure single-element STs is more challenging without the specifically shaped tectons providing directional intermolecular interactions [32,33]. In this work, by depositing Bi atoms on an InSb(111)B surface around 400 K, we have observed ST-like Bi films with a thickness of one to three monatomic layers (MLs) from our scanning-tunneling-microscope (STM) experiments. Our proposed theoretical model reveals that the formation of a Bi ST island requires an unusually large lattice mismatch between a monatomic Bi adlayer and substrate, relatively large adlayer-substrate and intra-adlayer elastic stiffnesses, and relatively weak intra-adlayer interatomic interactions. This formation mechanism essentially differs from that of the supramolecular STs synthesized previously.

In addition, it has been predicted theoretically that an ultrathin Bi film exhibits a stable nontrivial topological property [34–36], which makes the investigations of heteroepitaxial growth of ultrathin Bi films fundamentally interesting. Experiments have demonstrated the existence

of nontrivial topological edge states of single Bi(111) bilayer grown on Bi_2Te_3 films [37], as well as coexistence of topological edge state and superconductivity of Bi(111) ultrathin film grown on the $NbSe_2$ superconducting substrate [38]. Theoretical prediction of high-temperature quantum-spin-Hall state in an epitaxial Bi layer (called "bismuthene") grown on semiconductor substrates [39–41] has been recently confirmed experimentally for a SiC substrate [42]. A possible realization of topological high-temperature superconductivity in a hybrid of Bi(110) ultrathin film and copper oxide superconductor has been also reported recently [43]. Therefore, it is of interest to assess if the electronic topology is retained in ST Bi films.

The most common phase of a Bi bulk crystal is the α-As structure, the geometric parameters for which and Bi(111) film surface structure are shown in Supplemental Material, Fig. S1 [44]. Bulk InSb has a zinc blende structure. An InSb(111) surface with In termination is often called InSb(111)A surface, while an InSb($\bar{1}\,\bar{1}\,\bar{1}$) surface with Sb termination is often called InSb(111)B surface. The structure parameters for bulk InSb and (111) surfaces are shown in Fig. S2. An InSb(111)B surface can exhibit (3×3), (2×2), or (3×1) reconstruction, depending on the experimental conditions [58–65]. In our experiments, a smooth InSb(111)B surface is produced following an ultrahigh-vacuum (UHV) cleaning process (see Supplemental Material, Sec. S1 for details [44]). STM, reflection high-energy electron diffraction (RHEED), and two-dimensional fast-Fourier-transform (2D FFT) measurements indicate that the InSb(111)B surface is (3×3) reconstructed (see Supplemental Material, Fig. S3 [44]). For the (3×3)-reconstructed InSb(111)B surface, a currently accepted model is that proposed by Wever *et al.* in 1994, where the reconstructed top layer was determined to be composed of three types of In-Sb hexamers: α, β, and γ rings, from their x-ray diffraction and STM analyses [61]. This model also reasonably agrees with other experimental observations [60,64,65]. These conclusions are generally consistent with our STM results in Fig. S3 [44].

In our experiments, we deposit Bi atoms to a desired coverage θ (in units of ML; see Sec. S1 [44]) on the prepared InSb(111)B substrate surface (as described above) at a temperature T_{dep}. After deposition, we quench the system to room temperature with a total cooling time of t_{cool}. We measure the STM images at the liquid helium temperature of about 4 K. For more STM measurement details, see Sec. S1 [44].

The STM images in Figs. 1(a) and 1(b) show typical ST-like Bi films or islands formed on InSb(111)B surface at $\theta \approx 2$ ML, where different island height levels: 0, S_1, 2, S_3, 4, and B from lower to higher, are labeled. For a clearer view, these levels are plotted into a schematic in Fig. 1(c). Corresponding to the blue, red, and pink lines A, B, and C in Fig. S1(b) [44], the height profiles are shown in Figs. 1(d)–1(f), respectively. Level 0 is assumed to be a wetting layer composed of Bi, Sb, and In atoms by considering the (3×3) reconstruction of InSb(111)B surface (as described above) before deposition. As analyzed below, level S_1 corresponds to a ST-like 1-ML Bi on the wetting layer, level 2 to a 2-ML Bi, and level S_3 to a ST-like 1-ML Bi on 2-ML Bi. From our STM measurements (e.g., see Fig. 2, and Supplemental Material Figs. S4–S6 [44]), the regions of level 2 are (2×2)-reconstructed or disordered (see Sec. S3.5 [44]). Level 4 has a low occurrence statistically and is expected to be of 4-ML Bi (see analyses below). We label the higher bulklike islands than level 4 as level B.

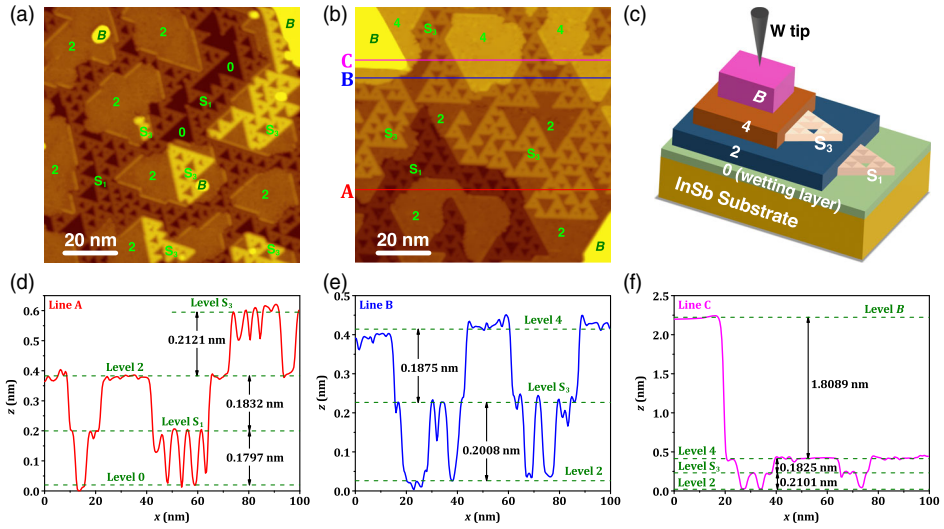

FIG. 1. (a),(b) STM images of typical ST-like Bi islands formed on InSb(111)B substrate at $\theta \approx 2$ ML. See Sec. S1 for details. (c) Schematic for different island height levels corresponding to the labels in (a),(b). (d),(e),(f) Height profiles for red, blue, and pink lines A, B, and C in (b), respectively.

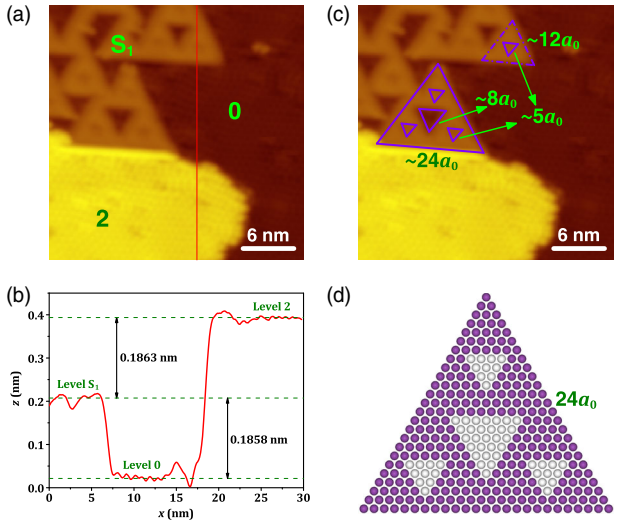

FIG. 2. (a) STM image at $\theta \approx 1$ ML. See Supplemental Material, Sec. S1 [44] for details. (b) Height profile for a red line in (a). (c) The same image as (a). Side lengths of STs are indicated. (d) Atomistic structure model for a 1-ML Bi ST with all side lengths accurately matching the lengths measured in (c). A purple ball denotes a lattice site occupied by a Bi atom and a gray ball denotes an unoccupied lattice site.

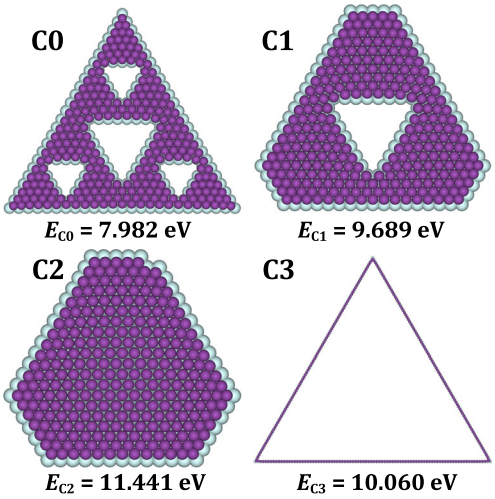

FIG. 3. Shapes and energies of four configurations after energy minimization for 1-ML Bi islands with the same number of Bi atoms, $N = 267$. A purple ball represents a Bi atom and a light ball represents a lattice point below this Bi atom. For $C0$, $C1$, and $C2$, $b = b_{1\,\mathrm{ML}} = 0.3304$ nm, $k_2 = k_{1\,\mathrm{ML}} = 766$ eV/nm^2, and $\phi = \phi_{1\,\mathrm{ML}} = -0.747$ eV; for $C3$, $b = b_{\mathrm{chain}} = 0.2865$ nm, $k_2 = k_{\mathrm{chain}} = 814$ eV/nm^2, and $\phi = \phi_{\mathrm{chain}} = -1.638$ eV; for all, $l = a_0 = 0.45816$ nm and $k_1 = k_{\mathrm{sub}} = 307$ eV/nm^2.

To model the atomistic structure of ST-like islands, we measure various side lengths of STs. The measured typical STs are shown in Fig. 2(a), where $\theta \approx 1$ ML. There are three height levels for this coverage, as shown by the line scan in Fig. 2(b). The height differences from level 0 to S_1 or from S_1 to 2 are about 0.186 nm, which is consistent with the values around 0.18 nm at $\theta \approx 2$ ML in Fig. 1(d). In Fig. 2(c), we highlight various side lengths of STs by purple lines, e.g., for a large ST, three longest side lengths are about $24a_0$ and the three side lengths of the inner larger vacancy triangle are about $8a_0$, while each of side lengths of three inner smallest vacancy triangles are about $5a_0$, where $a_0 = 0.458\,16$ nm is the InSb(111) plane lattice constant from experiments [66–68]. For the dashed triangle, each side length is about $12a_0$. That is, all these side lengths are approximately equal to integer multiples of a_0. Thus, a model for the atomistic structure of a ST Bi island can be obtained with the side lengths which can accurately match our experimental measurements, as illustrated in Fig. 2(d). Here, it should be also noted that the above side lengths are statistically representative values based on analysis of multiple STs from our STM images.

It is important to point out that the above STM analysis indicates that the nominal 1-ML Bi film has a huge lattice mismatch (>30%) with the substrate, as described below. Therefore, the film is unlikely to grow coherently rather forming extended defects to relieve strain. Instead of a normal mechanism of forming dislocations, islands, or voids [69,70], a novel unique strain relief mechanism via formation of ST-like structure is revealed, as elaborated below. Specifically, for a 1-ML Bi island with N Bi atoms on a substrate with a surface lattice parameter l, the total energy can be expressed as $E_{\mathrm{total}} = E_{\mathrm{electronic}} + E_{\mathrm{elastic}}^{\mathrm{Bi-sub}} + E_{\mathrm{elastic}}^{\mathrm{Bi-Bi}}$, based on a generic form of Frenkel-Kontrova-type Hamiltonian for elastic relaxations in bulk alloys [71] (for three terms, see Sec. S2.1 [44]). Considering the measured side lengths for STs in Fig. 2, we reasonably assume that the underlying InSb(111)B substrate has a triangular lattice with $l = a_0 = 0.458\,16$ nm at the interface. Other model parameters include spring parameters k_1 (adlayer-substrate) and k_2 (intra-adlayer), effective interaction parameter ϕ, and equilibrium adlayer lattice parameter b (see Sec. S2 [44]).

Consider four configurations with $N = 267$ in Fig. 3. $C0$ corresponds to the ST in Fig. 2(d). In principle, one can assess the thermodynamic stability of $C0$ by constructing a large number of configurations with the same N and then comparing their energies with $C0$ after energy minimization. However, analysis of just few judiciously selected configurations is sufficiently informative. We choose $C1$, $C2$, and $C3$. For $C1$, only the larger void in the middle remains relative to $C0$ and the three smaller voids around it are filled by truncating three ST edges to retain 267 atoms. For $C2$, we consider the limit of a compact island without any voids retaining 267 atoms. For $C3$, we consider the *opposite* limit to $C2$, where a single large void is bordered by three Bi monatomic chains. The energies of other configurations are expected to be between these limiting cases.

In contrast to $C3$, the configurations $C0$, $C1$, and $C2$ all involve portions of complete compact 1-ML Bi film.

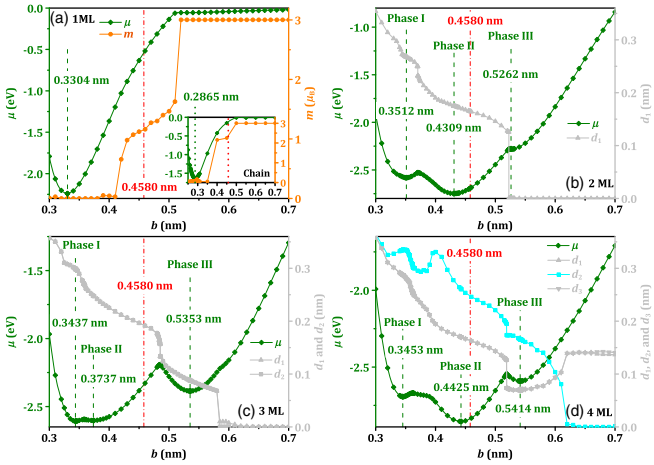

FIG. 4. DFT chemical potentials μ (the energy per Bi atom relative to gas phase) versus lateral lattice parameter b for freestanding (a) 1-, (b) 2-, (c) 3-, and (4) 4-ML Bi slabs. Interlayer spacings (d_1, d_2, and d_3) for 2-, 3-, and 4-ML slabs, as well as magnetic moments m for 1 ML in (a) and chain in the inset of (a), are also plotted. For details, see Sec. S3.2.

This motivates selecting the same set of parameters for them: $b = b_{1\,\mathrm{ML}} = 0.3304\,\mathrm{nm}$, $k_2 = k_{1\,\mathrm{ML}} = 766\ \mathrm{eV/nm^2}$, and $\phi = \phi_{1\,\mathrm{ML}} = -0.747$ eV. $b_{1\,\mathrm{ML}}$ is the DFT equilibrium lattice parameter for complete freestanding 1-ML Bi film [see Fig. 4(a)] and significantly less than a_0. Therefore, the nominal 1-ML Bi film has a huge tensile strain $\varepsilon = 38.67\%$ relative to a_0. $k_{1\,\mathrm{ML}}$ and $\phi_{1\,\mathrm{ML}}$ are estimated from our DFT calculations for the 1-ML Bi. $C3$ is made up of three monatomic Bi chains with an only slight deviation from the chain shape at each vertex, so we approximately take the parameters to be $b = b_{\mathrm{chain}} = 0.2865$ nm, $k_2 = k_{\mathrm{chain}} = 814\ \mathrm{eV/nm^2}$, and $\phi = \phi_{\mathrm{chain}} = -1.638$ eV. b_{chain} is the DFT equilibrium lattice parameter for infinite Bi chain [see the inset of Fig. 4(a)]. k_{chain} and ϕ_{chain} are estimated from our DFT calculations for the Bi chain. We also take $k_1 = k_{\mathrm{sub}} = 307\ \mathrm{eV/nm^2}$, which is a typical value estimated from our DFT calculations. Using these parameters (see Supplemental Material, Sec. S3 [44] for estimating all parameters) as input, we obtain the optimized energies per Bi atom, $E = E_{\mathrm{total}}/N$, which are $E_{C0} = 7.982$ eV, $E_{C1} = 9.689$ eV, $E_{C2} = 11.441$ eV, and $E_{C3} = 10.060$ eV for the four shapes, and then $E_{C0} < E_{C1} < E_{C3} < E_{C2}$. Thus, $C0$ is energetically most favorable, while the most compact $C2$ is least favorable. To examine how the results depend on the parameters k_1, k_2, ϕ, and b, we plot E versus the specific parameters r_k, r_ϕ, and b in Fig. S7 [44]. Briefly, the above conclusion remains for varying k_1 and k_2, or ϕ, in reasonable ranges. For b, we find a critical value $b_c \approx 0.4271$ nm (corresponding to a tensile strain $\varepsilon_c \approx 7.27\%$), i.e., $C0$ is more favorable than $C1$ and $C2$ for $b < b_c$ (or $\varepsilon > \varepsilon_c$), and unfavorable relative to $C1$ and $C2$ for $b > b_c$ (or $\varepsilon < \varepsilon_c$). See Sec. S2.3 [44] for details. Therefore, our key finding is that $C0$ affords more efficient strain relief than $C1$ and $C2$ for larger mismatch strain.

To understand the height levels observed in experiments, we perform DFT calculations for freestanding 1- to 4-ML Bi slabs with thicknesses $L = 1$ to 4. We find three phases (energy minima) for $L = 2$, 3, or 4 in the range of lateral lattice parameter b from 0.3 to 0.7 nm versus only one energy minimum for $L = 1$, as shown in Fig. 4. The existence of these local energy minima reflects the competition between van der Waals and covalent interactions with varying lateral and vertical Bi-Bi distances (b and interlayer spacings d_1, d_2, and/or d_3). The most-stable phases for $L = 1$ to 4 have the equilibrium lattice parameters $b_{1\,\mathrm{ML}} = 0.3304$ nm, $b_{2\,\mathrm{ML}} = 0.4309$ nm, $b_{3\,\mathrm{ML}} = 0.3437$ nm, and $b_{4\,\mathrm{ML}} = 0.4425$ nm, respectively.

Based on the DFT surface energies γ (Table S1 [72]), the stability order is $L = 2$, 4, 1, and 3, i.e., even-L slabs are much more stable than odd-L slabs. $\gamma_{L=1} = 4.091\ \mathrm{eV/nm^2}$ is relatively high, so the compact 1-ML Bi ($C2$) is not observed in STM images. Instead, the more stable 1-ML ST Bi island ($C0$) forms as level S_1 due to inhibited interlayer transport (level S_1 is metastable relative to level 2; see Sec. S3.5 [44]), as analyzed above. Level 2 corresponds to $L = 2$, which is the most-stable thickness due to the lowest $\gamma_{L=2} = 1.654\ \mathrm{eV/nm^2}$, and therefore this level has a high occurrence rate in STM images. In contrast, level 4 corresponding to $L = 4$ has a very low occurrence rate in STM images (see, e.g., Fig. 1) because $\gamma_{L=4} = 1.885\ \mathrm{eV/nm^2}$ is slightly higher than $\gamma_{L=2} = 1.654\ \mathrm{eV/nm^2}$, while $\gamma_{L=3} = 5.961\ \mathrm{eV/nm^2}$ is much higher so that 3-ML Bi is unobservable. Level B mainly corresponds to even-L Bi islands with $L > 4$. In addition, metastable phases in Fig. 4 are not generally expected to be observed in experiments. For more stability-analysis details of Bi films, see Sec. S3 [44].

Level S_3 has a significantly high occurrence rate. We interpret this level as a 1-ML ST-like Bi film forming on a superstable 2-ML Bi film, where the nominal 1-ML Bi film has a strain $\varepsilon = 30.42\%$ relative to $l = b_{2\,\mathrm{ML}} = 0.4309$ nm. This strain is also sufficiently large to form 1-ML ST Bi islands on a 2-ML Bi film. As listed in Supplemental Material, Table S2 [44], $C0$ (corresponding to level S_3) is always more favorable than the compact island $C2$ (corresponding to 3-ML Bi) as long as k_1 is not too small. Relative to 3-ML film with $l = b_{3\,\mathrm{ML}} = 0.3437$ nm, 1-ML Bi film has a small strain $\varepsilon = 4.03\%$, and then $C0$ is generally more unfavorable than other shapes (see Table S2 [44] again), i.e., forming ST-like structures on 3-ML Bi film is impossible. Relative to 4-ML (∞-ML) film with $l = b_{4\,\mathrm{ML}}(b_{\infty\,\mathrm{ML}}) = 0.4425(0.4546)$ nm, 1-ML Bi film has a large strain $\varepsilon = 33.93\%(37.59\%)$. However, we expect that k_1 would be significantly reduced with increasing $L > 2$ due to the adlayer Bi is far away from the InSb surface (see Sec. 3.4 [44]). Too small k_1 does not favor formation of ST structure but favor $C2$ (see Table S2 [44]) i.e., forming ST-like structures on 4-ML (∞-ML) Bi film would be unlikely. Instead, level B basically reverts to conventional

homoepitaxy, where the solid triangular islands grow with well-known properties [72] (see, e.g., Fig. S5).

Although we do not include InSb substrate in our DFT calculations, it is informative to compare DFT interlayer spacings in Fig. 4 with height levels in Fig. 1. The height difference between level S_1 and 2 is 0.1832 nm, reasonably consistent with $d_1 = 0.1751$ nm of 2-ML film (phase II). The height difference between level S_1 and 4 is about 0.58 nm, reasonably consistent with $d_1 + d_2 + d_3 = 0.6009$ nm of 4-ML film (phase II). The height difference between level S_1 and S_3 is about 0.39 nm, which happens to be close to Bi bulk $d = 0.4091$ nm.

Finally, we examine electronic topological properties of ST films. Our DFT analysis first demonstrates that free-standing 1- and 3-ML Bi films are topologically trivial, while 2- and 4-ML Bi are topologically nontrivial, consistent with previous predictions [35,36]. Then we perform an electronic structure analysis for a 5×5 supercell with one or seven Bi atoms removed from top Bi ML and find that such configurations are topologically trivial. Thus, a ST Bi film observed in our experiments is likely to be topologically trivial and consequently turn off the topology of nontrivial 2- or 4-ML Bi film. For details, see Sec. S3.7.

In summary, we have realized Bi ST structures grown on InSb(111)B surface. This is the first observation of single-element STs self-assembling on a semiconducting surface. Our STM measurements and theoretical analyses suggest that a ST ML as an adlayer can form on a wetting layer or 2-ML Bi film. The formation of ST structures requires a specifically large adlayer-substrate lattice mismatch (with tensile strain), sufficiently strong adlayer-substrate and intra-adlayer elastic stiffnesses, and sufficiently weak intra-adlayer interatomic interactions. Such fractal ST structures, as observed in our experiments, are expected to be able to turn off the electronic topology of Bi films. Such a feature could potentially provide a controllable way to tune the topological property in a quantum-spin-Hall thin film. This could make the system attractive to explore controlled Majorana Fermion formation for realizing topological quantum computing.

C. L., G. W., Y. Y., C. L., H. H., D. G., Y. L., S. W., H. Z., C. L., and J. J. thank the Ministry of Science and Technology of China (Grants No. 2019YFA0308600, No. 2020YFA0309000, No. 2016YFA0301003, and No. 2016YFA0300403), NSFC (Grants No. 11521404, No. 11634009, No. 92065201, No. 11874256, No. 11874258, No. 12074247, No. 11790313, and No. 11861161003), the Strategic Priority Research Program of Chinese Academy of Sciences (Grant No. XDB28000000), and the Science and Technology Commission of Shanghai Municipality (Grants No. 2019SHZDZX01, No. 19JC1412701, and No. 20QA1405100) for partial support. Y. H. was supported by the Materials Sciences and Engineering Division of the U.S. Department of Energy (USDOE) Office of Science Basic Energy Sciences, and the research was performed at the Ames Laboratory operated by Iowa State University under Contract No. DE-AC02-07CH11358. J. W. E. was supported by the NSF Project No. CHE-1507223. Y. Z. and F. L. were supported by the USDOE Office of Science Basic Energy Sciences under Grant No. DE-FG02-04ER46148. DFT calculations were performed with the Extreme Science and Engineering Discovery Environment (XSEDE), which is supported by the National Science Foundation under Grant No. ACI-1548562, and also used resources of the National Energy Research Scientific Computing Center (NERSC), a USDOE Office of Science User Facility operated under Contract No. DE-AC02-05CH11231.

*Corresponding author.
y27h@ameslab.gov
†Corresponding author.
jfjia@sjtu.edu.cn

[1] W. Sierpiński, C. R. Acad. Sci. **160**, 302 (1915), https://gallica.bnf.fr/ark:/12148/bpt6k31131/f302.item.
[2] F. Hausdorff, Math. Ann. **79**, 157 (1918).
[3] E. Conversano and L. T. Lalli, Aplimat J. Appl. Math. **4**, 113 (2011), http://www.aplimat.com/index.php/aplimat-archive/volume-4.
[4] S. Wolfram, Am. Math. Mon. **91**, 566 (1984).
[5] D. G. Poole, Math. Mag. **67**, 323 (1994).
[6] M. F. Barnsley, *Fractals Everywhere*, 2nd ed. (Academic Press, New York, 1993), https://www.elsevier.com/books/fractals-everywhere/barnsley/978-0-12-079061-6.
[7] S. Wolfram, Rev. Mod. Phys. **55**, 601 (1983).
[8] P. W. K. Rothemund, N. Papadakis, and E. Winfree, PLOS Biol. **2**, e424 (2004).
[9] J. I. Lathrop, J. H. Lutz, and S. M. Summers, Theor. Comput. Sci. **410**, 384 (2009).
[10] J. Kou, Y. Liu, F. Wu, J. Fan, H. Lu, and Y. Xu, J. Appl. Phys. **106**, 054905 (2009).
[11] J. A. Fan, W.-H. Yeo, Y. Su, Y. Hattori, W. Lee, S.-Y. Jung, Y. Zhang, Z. Liu, H. Cheng, L. Falgout *et al.*, Nat. Commun. **5**, 3266 (2014).
[12] E. van Veen, S. Yuan, M. I. Katsnelson, M. Polini, and A. Tomadin, Phys. Rev. B **93**, 115428 (2016).
[13] K Wang, Y. Liu, and T. Liang, Physica (Amsterdam) **498B**, 33 (2016).
[14] M. Brzezińska, A. M. Cook, and T. Neupert, Phys. Rev. B **98**, 205116 (2018).
[15] D. F. Nicola, N. S. P. Purayil, D. Spirito, M. Miscuglio, F. Tantussi, A. Tomadin, F. D. Angelis, M. Polini, R. Krahne, and V. Pellegrini, ACS Photonics **5**, 2418 (2018).
[16] Y. Wang, N. Xue, R. Li, T. Wu, N. Li, S. Hou, and Y. Wang, ChemPhysChem **20**, 2262 (2019).
[17] H. Huang and F. Liu, Phys. Rev. Lett. **121**, 126401 (2018).
[18] H. Huang and F. Liu, Phys. Rev. B **98**, 125130 (2018).
[19] S. L. Tait, Nat. Chem. **7**, 370 (2015).
[20] R. Sarkar, K. Guo, C. N. Moorefield, M. J. Saunders, C. Wesdemiotis, and G. R. Newkome, Angew. Chem., Int. Ed. Engl. **53**, 12182 (2014).

[21] J. Shang, Y. Wang, M. Chen, J. Dai, X. Zhou, J. Kuttner, G. Hilt, X. Shao, J. M. Gottfried, and K. Wu, Nat. Chem. **7**, 389 (2015).

[22] X. Zhang, N. Li, L. Liu, G. Gu, C. Li, H. Tang, L. Peng, S. Hou, and Y. Wang, Chem. Commun. **52**, 10578 (2016).

[23] X. Zhang, N. Li, G.-C. Gu, H. Wang, D. Nieckarz, P. Szabelski, Y. He, Y. Wang, C. Xie, Z.-Y. Shen *et al.*, ACS Nano **9**, 11909 (2015).

[24] N. Li, X. Zhang, G.-C. Gu, H. Wang, D. Nieckarz, P. Szabelski, Y. He, Y. Wang, J.-T. Lü, H. Tang *et al.*, Chin. Chem. Lett. **26**, 1198 (2015).

[25] Q. Sun, L. Cai, H. Ma, C. Yuan, and W. Xu, Chem. Commun. **51**, 14164 (2015).

[26] A. Rastgoo-Lahrood, N. Martsinovich, M. Lischka, J. Eichhorn, P. Szabelski, D. Nieckarz, T. Strunskus, K. Das, M. Schmittel, W. M. Heckl, and M. Lackinger, ACS Nano **10**, 10901 (2016).

[27] G. Gu, N. Li, L. Liu, X. Zhang, Q. Wu, D. Nieckarz, P. Szabelski, L. Peng, B. K. Teo, S. Hou *et al.*, RSC Adv. **6**, 66548 (2016).

[28] N. Li, G. Gu, X. Zhang, D. Song, Y. Zhang, B. K. Teo, L. Peng, S. Hou, and Y. Wang, Chem. Commun. **53**, 3469 (2017).

[29] C. Li, X. Zhang, N. Li, Y. Wang, J. Yang, G. Gu, Y. Zhang, S. Hou, L. Peng, K. Wu *et al.*, J. Am. Chem. Soc. **139**, 13749 (2017).

[30] S. N. Kempkes, M. R. Slot, S. E. Freeney, S. J. M. Zevenhuizen, D. Vanmaekelbergh, I. Swart, and C. M. Smith, Nat. Phys. **15**, 127 (2019).

[31] Y. Mo, T. Chen, J. Dai, K. Wu, and D. Wang, J. Am. Chem. Soc. **141**, 11378 (2019).

[32] D. Nieckarz and P. Szabelski, Chem. Commun. **50**, 6843 (2014).

[33] D. Nieckarz and P. Szabelski, Chem. Commun. **52**, 11642 (2016).

[34] S. Murakami, Phys. Rev. Lett. **97**, 236805 (2006).

[35] Z. Liu, C.-X. Liu, Y.-S. Wu, W.-H. Duan, F. Liu, and J. Wu, Phys. Rev. Lett. **107**, 136805 (2011).

[36] Z. F. Wang, L. Chen, and F. Liu, Nano Lett. **14**, 2879 (2014).

[37] F. Yang, L. Miao, Z. F. Wang, M.-Y. Yao, F. Zhu, Y. R. Song, M.-X. Wang, J.-P. Xu, A. V. Fedorov, Z. Sun, G. B. Zhang, and C. Liu, F. Liu, D. Qian, C. L. Gao, and J. F. Jia, Phys. Rev. Lett. **109**, 016801 (2012).

[38] H.-H. Sun, M.-X. Wang, F. Zhu, G.-Y. Wang, H.-Y. Ma, Z.-A. Xu, Q. Liao, Y. Lu, C.-L. Gao, Y.-Y. Li *et al.*, Nano Lett. **17**, 3035 (2017).

[39] M. Zhou, W. Ming, Z. Liu, Z. Wang, P. Li, and F. Liu, Proc. Natl. Acad. Sci. U.S.A. **111**, 14378 (2014).

[40] C.-H. Hsu, Z.-Q. Huang, F.-C. Chuang, C.-C. Kuo, Y.-T. Liu, H. Lin, and A. Bansil, New J. Phys. **17**, 025005 (2015).

[41] P. Li, M. Zhou, L. Zhang, Y. Guo, and F. Liu, Nanotechnology **27**, 095703 (2016).

[42] F. Reis, G. Li, L. Dudy, M. Bauernfeind, S. Glass, W. Hanke, R. Thomale, J. Schäfer, and R. Claessen, Science **357**, 287 (2017).

[43] N. Shimamura, K. Sugawara, S. Sucharitakul, S. Souma, K. Iwaya, K. Nakayama, C. X. Trang, K. Yamauchi, T. Oguchi, K. Kudo *et al.*, ACS Nano **12**, 10977 (2018).

[44] See Supplemental Material at http://link.aps.org/supplemental/10.1103/PhysRevLett.126.176102 for crystalline structures, STM measurement, model details, DFT calculation details, additional data, and additional discussions, which includes Refs. [45–57].

[45] Y. Han, D.-J. Liu, and J. W. Evans, Nano Lett. **14**, 4646 (2014).

[46] W. Li, L. Huang, J. W. Evans, and Y. Han, Phys. Rev. B **93**, 155416 (2016).

[47] W. Li, L. Huang, R. G. S. Pala, G.-H. Lu, F. Liu, J. W. Evans, and Y. Han, Phys. Rev. B **96**, 205409 (2017).

[48] G. Kresse and D. Joubert, Phys. Rev. B **59**, 1758 (1999).

[49] G. Kresse and J. Furthmüller, Phys. Rev. B **54**, 11169 (1996).

[50] J. Klimeš, D. R. Bowler, and A. Michaelides, J. Phys. Condens. Mat. **22**, 022201 (2010).

[51] Y. Han, K. C. Lai, A. Lii-Rosales, M. C. Tringides, J. W. Evans, and P. A. Thiel, Surf. Sci. **685**, 48 (2019).

[52] Y. Han, M. C. Tringides, J. W. Evans, and P. A. Thiel, Phys. Rev. Research **2**, 013182 (2020).

[53] W.-K. Huang, K.-W. Zhang, C.-L. Yang, H. Ding, X. Wan, and S.-C. Li, Nano Lett. **16**, 4454 (2016).

[54] A. A. Mostofi, J. R. Yates, Y.-S. Lee, I. Souza, D. Vanderbilt, and N. Marzari, Comput. Phys. Commun. **178**, 685 (2008).

[55] F. Ersan, E. Aktürk, and S. Ciraci, Phys. Rev. B **94**, 245417 (2016).

[56] W. Li, L. Huang, M. C. Tringides, J. W. Evans, and Y. Han, J. Phys. Chem. Lett. **11**, 9725 (2020).

[57] C. Kittel, *Introduction to Solid State Physics*, 7th ed. (John Wiley & Sons, New York, 1996).

[58] T. Nakada, T. Ikeda, M. Yata, and T. Osaka Surf. Sci. **222**, L825 (1989).

[59] T. Nakada and T. Osaka, Phys. Rev. Lett. **67**, 2834 (1991).

[60] L. Ö. Olsson, J. Kanski, L. Ilver, C. B. M. Andersson, M. Björkqvist, M. Göthelid, U. O. Karlsson, and M. C. Håkansson, Phys. Rev. B **50**, 18172 (1994).

[61] J. Wever, H. L. Meyerheim, W. Moritz, V. Jahns, D. Wolf, H. Schulz, L. Seehofer, and R. L. Johnson, Surf. Sci. **321**, L225 (1994).

[62] M. Björkqvist, M. Göthelid, L. Ö. Olsson, J. Kanski, and U. O. Karlsson, J. Vac. Sci. Technol. B **14**, 957 (1996).

[63] S. Cho, Y.-H. Um, Y. Kim, G. K. L. Wong, J. B. Ketterson, and J.-I. Hong, J. Vac. Sci. Technol. A **20**, 1191 (2002).

[64] K. Inada, R. Takahashi, N. Naruse, T. Kadohira, S.-P. Cho, and T. Osaka, J. Surf. Sci. Soc. Jpn. **24**, 105 (2003).

[65] J. Mäkelä, Z. S. J. Rad, J.-P. Lehtiö, M. Kuzmin, M. P. J. Punkkinen, P. Laukkanen, and K. Kokko, Sci. Rep. **8**, 14382 (2018).

[66] P. Cucka and C. S. Barrett, Acta Cryst. **15**, 865 (1962).

[67] D. Schiferl and C. S. Barrett, J. Appl. Crystallogr. **2**, 30 (1969).

[68] I. Vurgaftman, J. R. Meyer, and L. R. Ram-Mohan, J. Appl. Phys. **89**, 5815 (2001).

[69] J. Tersoff and F. K. LeGoues, Phys. Rev. Lett. **72**, 3570 (1994).

[70] F. Liu and M. G. Lagally, Surf. Sci. **386**, 169 (1997).

[71] B. D. Krack, V. Ozoliņš, M. Asta, and I. Daruka, Phys. Rev. Lett. **88**, 186101 (2002).

[72] T. Michely and J. Krug, Islands, Mounds and Atoms, Springer Series in Surface Sciences Vol. **42**, https://link.springer.com/book/10.1007/978-3-642-18672-1.